

PROCEEDINGS OF SPIE

[SPIDigitalLibrary.org/conference-proceedings-of-spie](https://spiedigitallibrary.org/conference-proceedings-of-spie)

Printability and propagation of stochastic defects through a study of defects programmed on EUV mask

Poulomi Das, Alain Moussa, Christophe Beral, Mihir Gupta, Mohamed Saib, et al.

Poulomi Das, Alain Moussa, Christophe Beral, Mihir Gupta, Mohamed Saib, Sandip Halder, Anne Laure Charley, Philippe Leray, "Printability and propagation of stochastic defects through a study of defects programmed on EUV mask," Proc. SPIE 11854, International Conference on Extreme Ultraviolet Lithography 2021, 118540Z (19 October 2021); doi: 10.1117/12.2602034

SPIE.

Event: SPIE Photomask Technology + EUV Lithography, 2021, Online Only

Printability and propagation of stochastic defects through a study of defects programmed on EUV mask

Poulomi Das, Alain Moussa, Christophe Beral, Mihir Gupta, Mohamed Saib, Sandip Halder, Anne Laure Charley, Philippe Leray

Imec, Kapeldreef 75, 3001 Leuven Belgium

ABSTRACT

The feasibility of using extreme ultra violet (EUV) lithography in high volume manufacturing makes the technology a very strong candidate for sub 20nm patterning^{1,2}. However defect control remains a major challenge even today. The aim of this paper is to understand propagation of the programmed defects present on the EUV mask to wafer to get an understanding of how stochastic defects may evolve through processes and how we can mitigate it. The evolution of the defects from mask to wafer post lithography and post etch has been studied both theoretically by calculating change in defect area from a script on images taken with e-beam inspection and other metrology techniques like atomic force microscopy. The end goal is to study the propagation of these programmed defects from post lithography to post etch on wafer through parameters like defect area, defect sizes and stack height information[1][2].

Keywords: Stochastic defects, defect propagation, EUV mask, defect printability, AFM, SEM

1. INTRODUCTION

As we move to further critical dimension (CD) shrink with EUV lithography, monitoring how defects print on wafer has gained critical importance. Stochastic defects are those defects that emerge from pattern formation process itself. These defects are random, non-repeating and isolated [3] [4]. In order to study their propagation from lithography to etch on wafer, this paper makes an attempt to study and correlate propagation of defects – bridges that are programmed on an EUV mask.

For ease of demonstration, programmed defects on matrix are given a special nomenclature. For every type of defects on the matrix (A, B, C, D, E and F – Figure 1), the respective biggest defect per type is placed at location number 1 and the smallest defect is located at position 15. As we know, the programmed defects sizes decrease as we go right to left on each defect type. This means, in row A, for defect type A, the largest defect is called defect A1 and the smallest would be called A15.

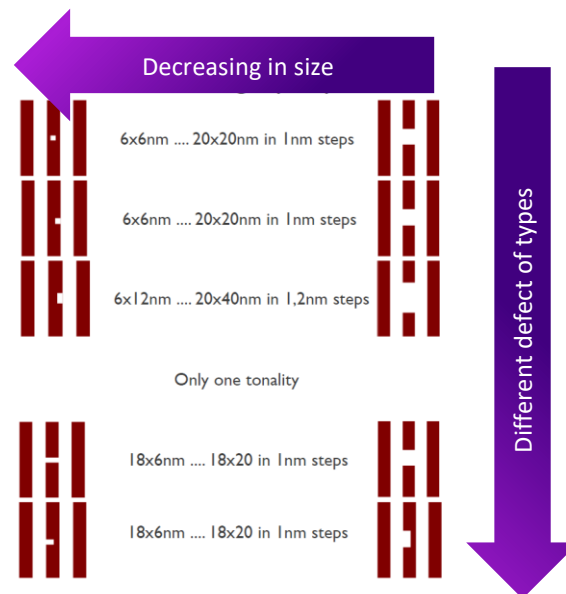


Figure 1: Defects programmed as bridges on mask design in a 15 x 10 matrix

2. EXPERIMENT & METHODOLOGY

The propagation of programmed defects from mask to post lithography to post etch at wafer level on wafers exposed on NXE:3400 EUV lithography module with a simple stack coated with a Chemically Amplified Resist (CAR) with an in-house defectivity mask, called Stoch16 was studied. On this mask, we focused on 32nm line/space pitch size, with mask bias of 14.5/17.5(17.5nm absorber lines on mask) (Figure 2). We focused on 5 different types of programmed defects with varying dimensions.

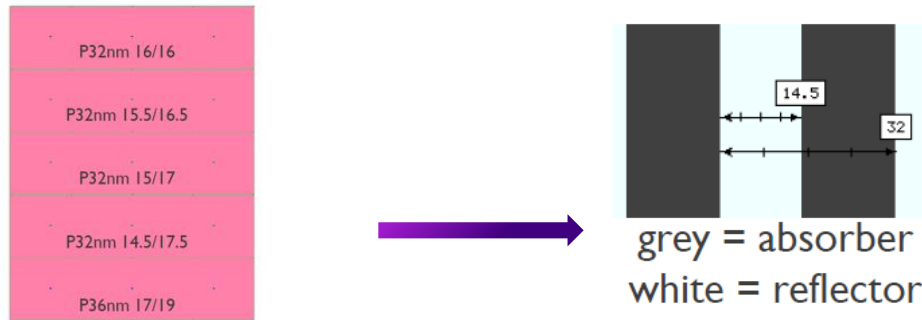


Figure 2: Layout of STOCH16 defectivity mask, focussing on 17.5 nm absorber lines on mask

The programmed defects are organized as a matrix of line bridges (bumps) in a 15x10 array distribution. The biggest line bridge has a size of 20x40nm decreasing down with a fixed step size for each defect type. The smallest line bridge has a size of 6x6nm (Figure 1).

For the study for these defect propagation, a standard imec Back-End-Of-Line stack has been used (Figure 3).

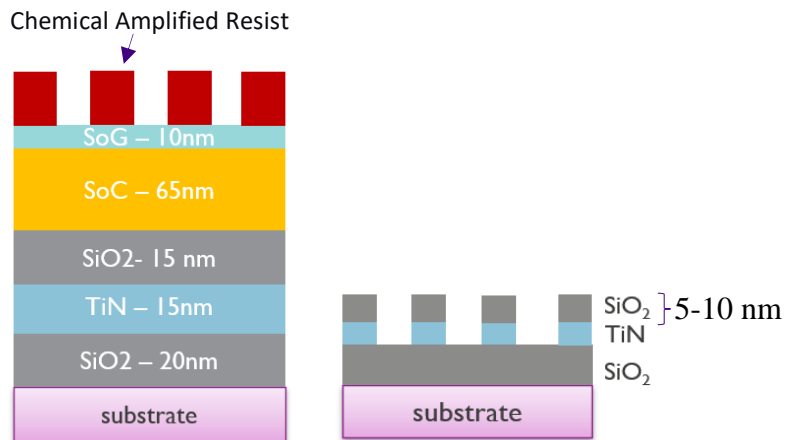


Figure 3: Stack post lithography development (left); Stack post etch (right)

Followed by this, CDSEM inspection is done on wafers at after development inspection (ADI) and at after etch inspection (AEI). This is done to be certain that dies picked from the wafer maps at ADI and AEI have as minimum litho-etch bias on CD. The study of defect propagation is deduced by studying the area of programmed defects at ADI and AEI. In step 1, top surface area of the programmed defects are calculated from SEM images and by creation of a script. Similarly the top area of these programmed defects is also calculated on the mask.

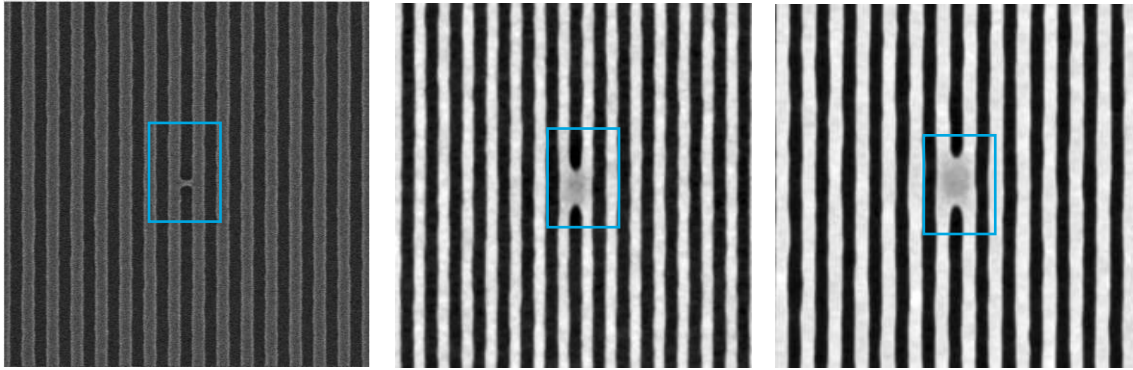


Figure 4: Example: Defect A1 on mask (left); on wafer ADI (center); on wafer AEI (right)

In figure 4, same defect A1 is imaged with SEM on mask , on wafer after lithography and as well as on wafer after etch. This is done for all 135 defects on 2 dies selected on wafer at ADI and AEI. Defect type D does not print for the given tonality of the resist, all the others are expected to bridge or form protrusions.

With SEM imaging on e-beam tool, images are collected with the programmed defects at the center of FoV for every defect type in the matrix (Figure 5-a). Then with help of a coded script, a “mask” is generated to highlight the programed defects at every location. This is achieved by overlayng the SEM image with the aforesaid mask which enhances the dark pixel to colour black and the light pixels to color white. Then the pixel intensity of the SEM image is averaged vertically. This results in a Overlaid SEM + Mask image (Figure 5-b). The overlaid image is then converted to a binary image by setting a threshold on the pixel intensity histogram (Figure 5-c). The top area of the programmed defect is finally calculated from the binary extracted image of the defect.

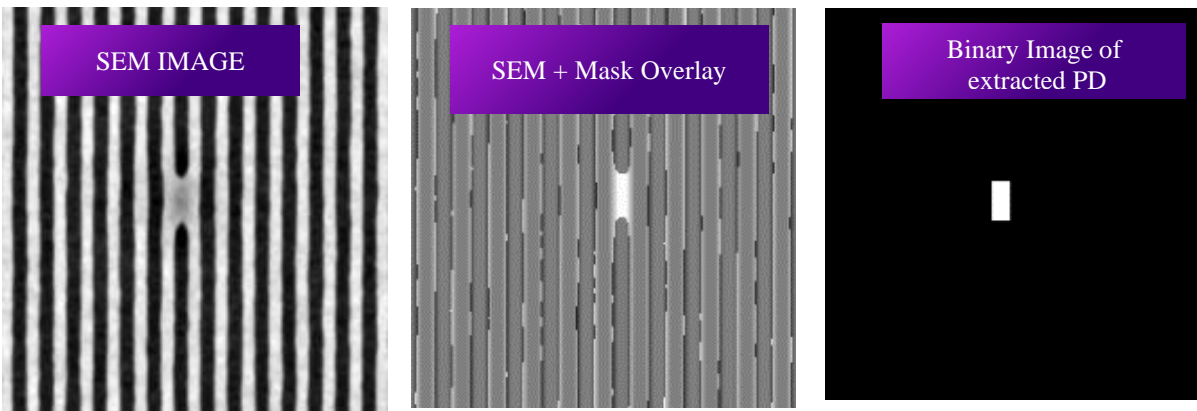


Figure 5: (a) SEM image taken on e-beam tool (left); (b) SEM image masked to create an overlay image (center); (c) An extracted binary image of the programmed defect (right)

A second, unusual technique has also been used to study the lateral area of the programmed defect with Atomic Force Microscopy (AFM). The AFM probe scans the line space arrays while it can capture the topography of the defect in z-direction. This scan is also done at ADI and AEI on the location of the programmed defects.

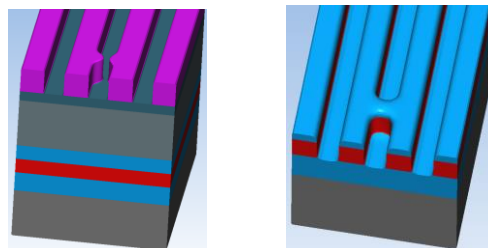


Figure 6: Coventor model generated on ADI stack (left) and AEI stack (right) where the height of the programmed defect between 2 adjacent lines is studied from top of resist line to the bottom

In figure 6, with coventor modelling with stack details at lithography and at etch, we can see how the programmed defect F9 looks at ADI from the lateral side and how it becomes a full bridge at AEI. This view got us intersted to investigate the lateral area. However, it is important to bear in mind that the topography height seen by the AFM probe in z-direction is highly affected by probe quality and size of the probe tip used.

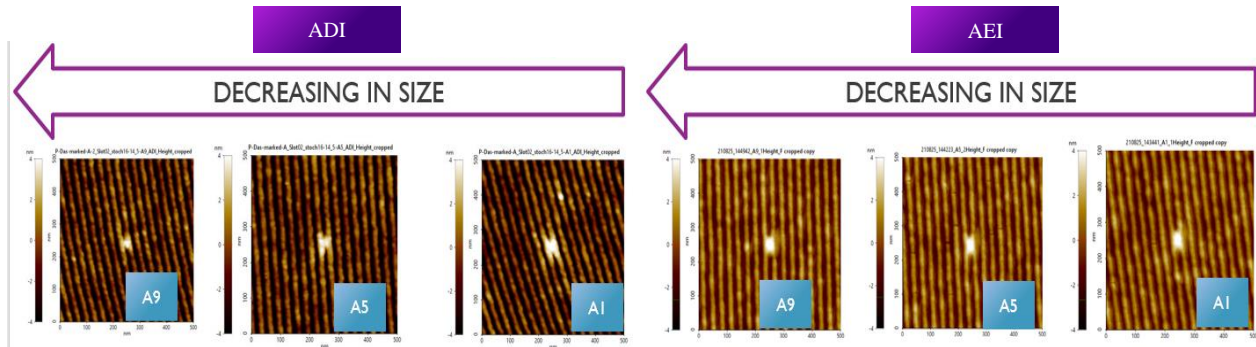


Figure 7: AFM scanned image of programmed defect A1, A5 and A9 at ADI and AEI

The decreasing programmed defect size as we move from A1 to A9 in figure 7 is noticed which reduces further as we go down to smaller defect sizes on the matrix.

3.RESULTS

Post ADI and AEI CDSEM inspections, a litho-etch mean CD bias of less than 0.5nm is observed (Figure 8). Select dies are chosen for the script and AFM based area analysis respectively.

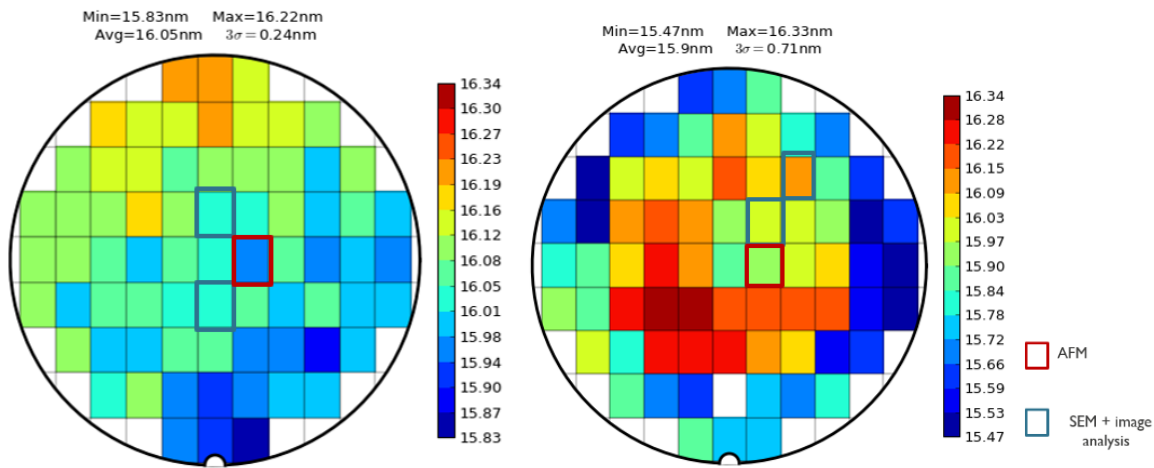


Figure 8: ADI v/s AEI CDSEM data with dies indicated that has been used for AFM and SEM + script-based analysis

As shown on figure 8 above , area propagation of the defects from mask to wafer after lithography and after etch is calculated and we reach the following correlation. Dies used at ADI and AEI area calculation is indicated (Figure 9).

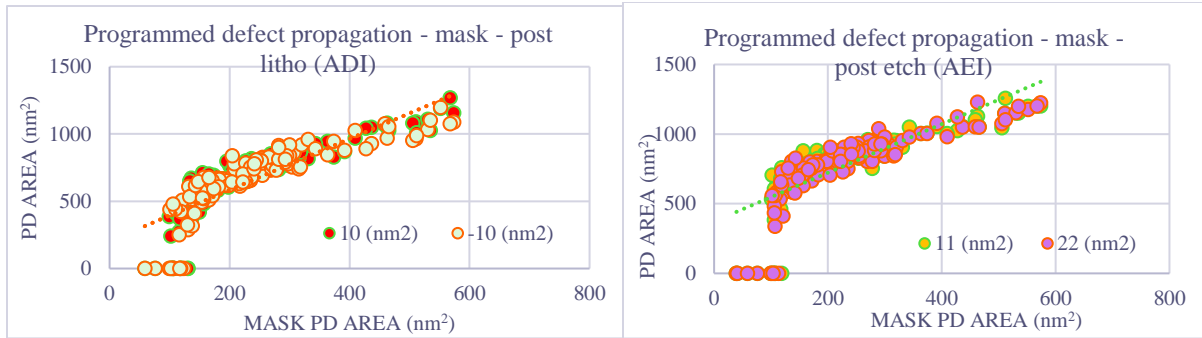


Figure 9: Propagation of area of programmed defects from mask to litho (left).
Propagation of area of programmed defects from mask to etch (right)

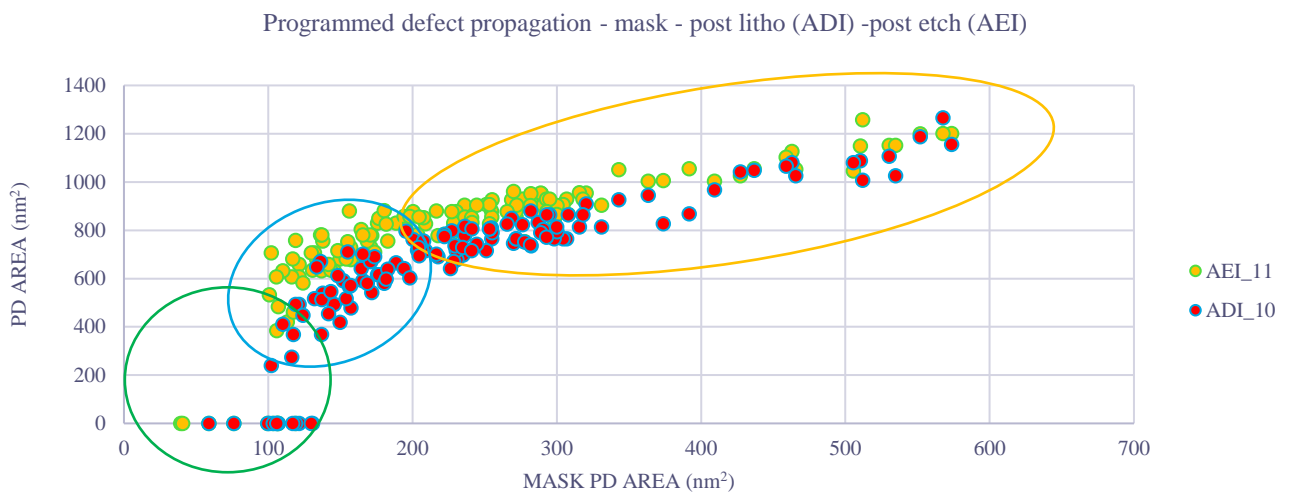
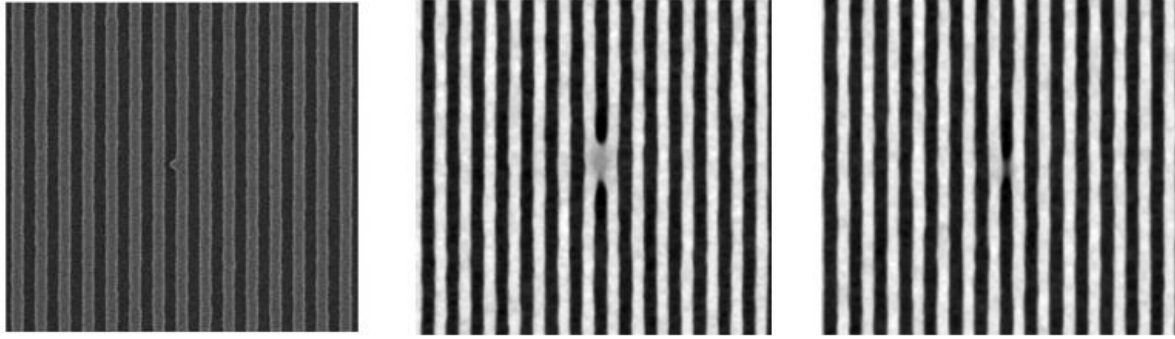


Figure 10: Area propagation from litho to etch across mask defect propagation

The size propagation from litho to etch is plotted against respective defect size propagation on mask (Figure 10). This gave us 3 distinct regimes. In the first “green” regime, it is seen that for mask defect sizes below 150 nm², ADI defects mostly would not print but the same defects at AEI could have varying printing tendency. In the second regime, “purple” regime, ADI defect sizes between 200 – 600 nm² will correspondingly becomes 400-800 nm² at AEI indicating a tendency of increasing defect size at AEI. Finally in the third, “yellow” regime, defects sizes increase from 600 – 1200 nm² at ADI to 700 – 1300 nm² at AEI.

However the above analysis derived from Figure 10, points to a very interesting tail region in the plot which falls within the green regime.

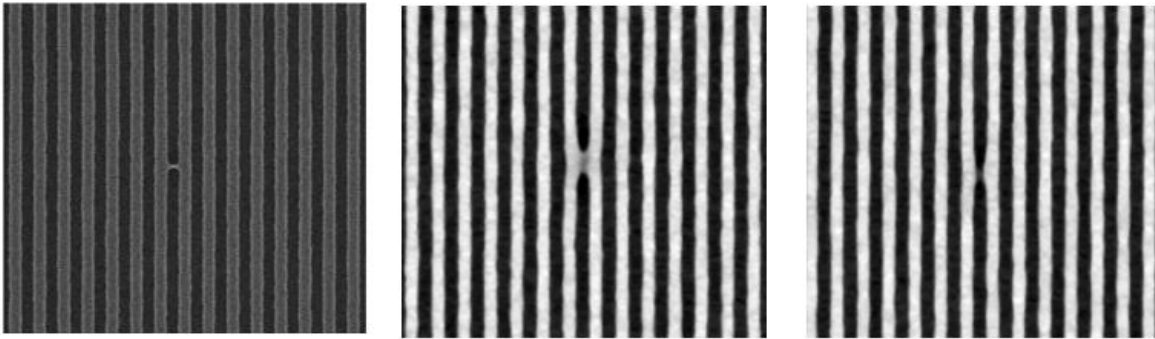
a



Defect Type F9 on mask Defect Type F9 on row 1 Die (1,0) Defect Type F9 on row 2 Die (1,0)



b



Defect Type F15 on mask Defect Type F15 on row 1 Die (1,0) Defect Type F15 on row 1 Die (-1,0)

Figure 11: Stochasticity in smallest type programmed defects

For continuing the study of the tail region, we take a look at defect type F for instance. There are 2 consecutive rows of defect F present on the design matrix separated by 10 um distance between F1 of row 1 and F1 of row 2 (Figure 11). In Figure 11 – a , F9 defect is a protrusion on mask and it becomes a full bridge at ADI wafer on row 1 however, on row 2 ADI on the same die, it's a protrusion or residue at the bottom of the resist line. Similarly, in Figure 11-b, defect F15 is a small full bridge on mask and becomes a full bridge at ADI on wafer in row 1 on die (1,0). However on row 1 of adjacent die(-1,0) on the same wafer with similar CD, defect becomes a protrusion. These two are some of several example that shows that smaller defects in the tail region show high stochasticity.





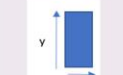



		Mask Dimension	ADI	AEI	Example	Image Mask	Image ADI wafer	Image AEI wafer
Type 1		$8\text{nm} < y < 14\text{nm}$	Partial bridge/residue	Will bridge (even if no bridge on ADI)	Defect F14			
Type 2		$x < 8\text{nm}$	No print	No print	Defect C15			

Table 1: Shows size-based limitation on smaller defects that print or not at ADI and/or AEI

Moving on to lateral area based defect propagation done with AFM, the goal is to calculate the area of the lateral side of the defect by subtracting the area under the double lines (2X32nm pitch) adjacent to the programmed defect, shown within region marked as “N” on either sides from the average area under a pair of adjacent lines in the FoV that contains the defect, shown within the regions marked “M”.

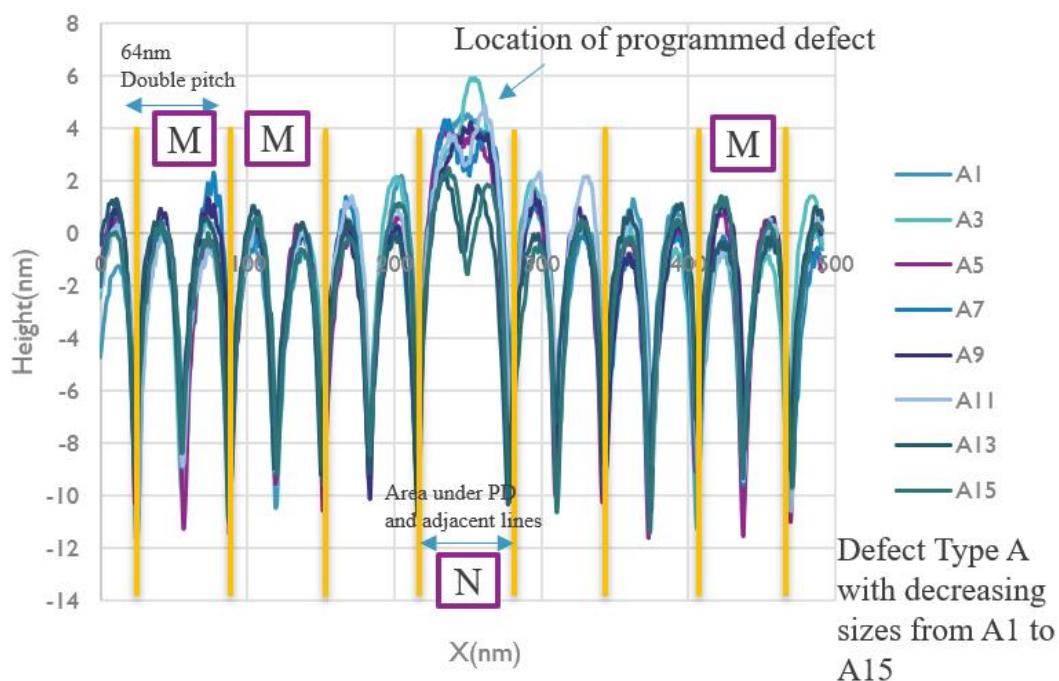


Figure 12: Plot generated from AFM scan generated raw data for all defect sizes for defect type A. Area N – Average area M gives the area of the lateral face of programmed defect

The highest point or bump in the plot above generated from raw AFM data indicates the location of the programmed defect between 2 lines (Figure 12).

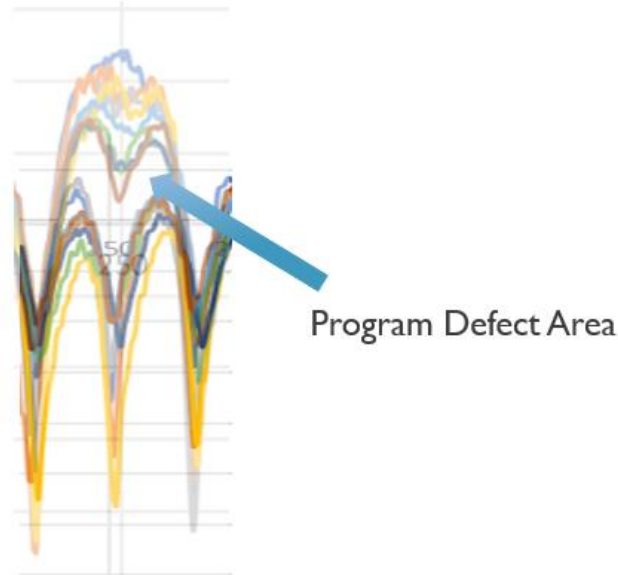


Figure 13: white area is the lateral area of PD is being studied

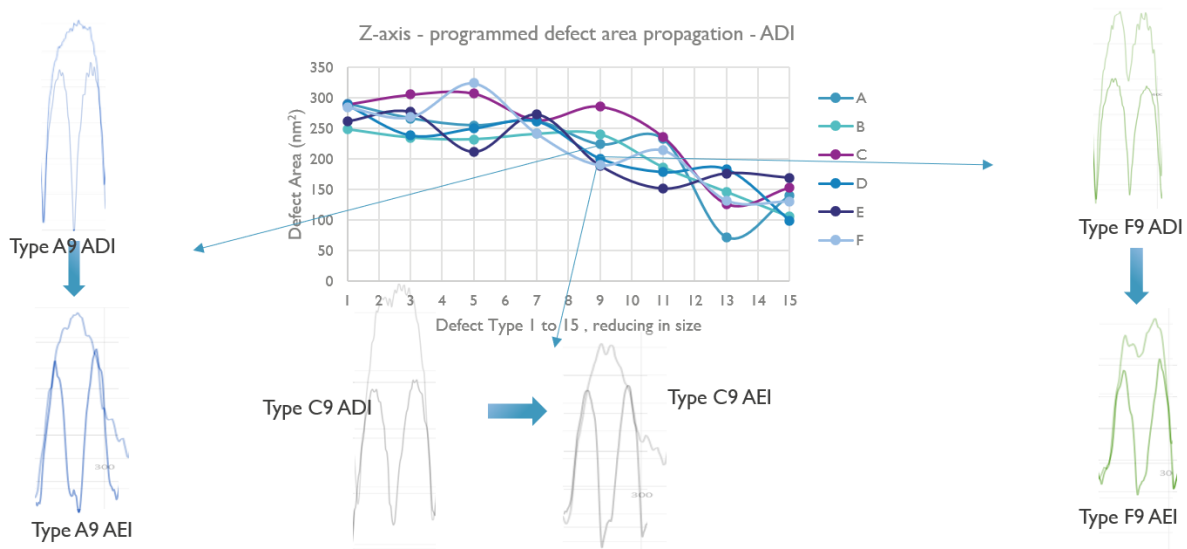


Figure 14: Area propagation on the lateral side of the defects s plotted at ADI and then at AEI

We have been able to map all defect types at ADI with AFM that showed a decreasing lateral area as we move from defect type 1 to type 15 across each type of defects. The ensuing reduction on lateral area observed at AEI only confirms the top oxide consumption post etch.

4. STRENGTH AND WEAKNESS – OUTLINE ON THE TECHNIQUE USED

Script analysis technique to calculate top area of defects is a fast technique once set up and be used to monitor wafers to robust data collection. However the minor con remains that this technique sometimes gives false negatives meaning if the is a tiny under bridge below resist line, the area would be flagged as not bridging. This needs to wisely accounted for in the script. Whereas the lateral area propagation with AFM has been very interesting to see change in defect size in the z-direction from ADI to AEI. The only weakness in the process remains the control of the quality and size of the AFM probe needs to be maintained.

Through this study , we have noticed that bridges become bigger post etch with CAR patterning. The smallest defect in tail region for certain defect types never print which is very interesting for us to analyze the minimum requirements for sensitivity of the optical defect inspection tool to detect these defects at ADI. We can also determine the critical size of defect on mask that will bridge at AEI.

With this study we could further try to combine the 2 techniqiue to dtermin the volume of defects in the next steps (x & y from SEM mimaging and height in z from AFM imaging) to understand if there is a volume limit above or below which stochastic defects will print or not at both ADI and AEI.

REFERENCES

- [1] Bonam R., Tien H, Chou A, et al; EUV Mask and Wafer Defectivity: Strategy and Evaluation for Full Die Defect Inspection; [2] Cho K, Park J, Park C, Lee Y, Kang I, Yeo J et al; The analysis of EUV mask defects using a wafer defect inspection system;
- [3] Sah K, Cross A, Plihal M, Vidyasagar A, Babulnath R, Fung D, De Bisscop P, Halder S; EUV stochastic defect monitoring with advanced broadband optical wafer inspection and e-beam review systems
- [4] De Biscchop P, Hendricks E; Stochastic printing failures in EUV lithography;
- [5] De Bisschop P, Van de Kerkhove, Mailfert J, Vaglio Pret A, Biafore J; Impact of stochastic effects on EUV printability limits

ACKNOWLEDGEMENT

I would like to thank imec colleagues Jeroen Van de Kerkhove and Victor Blanco for their collaboration on CD data study and stack simulation studies respectively.